Available online at www.sciencedirect.com
SCIENCE DIRECT
Engineering Fracture Mechanics 73 (2006) 537–552
Engineering Fracture Mechanics
www.elsevier.com/locate/engfracmech

Failure assessment diagram methods for strain-based fracture

P.J. Budden *

British Energy Generation Ltd., Plant Integrity Branch, Barnett Way, Barnwood, Gloucester GL4 3RS, UK

Received 3 May 2004; received in revised form 24 August 2005; accepted 29 September 2005
Available online 28 November 2005

Abstract

Stress-based fracture assessment procedures contain conservatism when assessing strain- or displacement-controlled loads in excess of yield. Alternative strain-based methods are discussed in this paper and compared with an existing approach in the R6 defect assessment procedure that allows reduction in conservatism for the case of fixed displacement or rotation loading. Published finite element results for semi-elliptical cracks in plates are re-interpreted as values of J against remote strain and used to assess recent strain-based estimates of J. An assessment procedure based on a strain-based failure assessment diagram is outlined.

Keywords: Fracture; Displacement control; Strain-based methods; J estimates

1. Introduction

The basic approach in fitness-for-service defect assessment procedures such as R6 [1] and BS7910 [2] involves consideration of the stresses acting on the flawed section. The stresses are evaluated from the loads on the uncracked structure by elastic calculation. However, this can lead to conservatism in the assessment of displacement-controlled or strain-controlled loads in excess of yield. Hence there has been renewed interest in strain-based methods [3–7] for particular applications. For example, in the oil and gas industries, welded pipelines can experience large deformations due to pipe reeling and laying or in service [5–7].

Strain- or displacement-based approaches are discussed in this paper, focussing on potential modifications to the basic R6 approach. Firstly, Section 2 describes the existing alternative approach in Section III.14 of R6, which addresses the case of fixed displacement or rotation loading. Stresses are calculated which account for the compliance changes due to plasticity and the presence of the crack. This can result in enhanced margins in an assessment using the R6 failure assessment diagram (FAD). Subsequently, Linkens et al. [3] have defined a general strain-based approach, termed the reference strain method (RSM), which directly estimates the crack driving force J from the applied, uncracked-body strain field for small cracks. The approach is compatible

* Tel.: +44 1452 653824; fax: +44 1452 653025.
E-mail address: peter.budden@british-energy.com

0013-7944/$ - see front matter © 2005 Elsevier Ltd. All rights reserved.
doi:10.1016/j.engfracmech.2005.09.008

Nomenclature

a, a_{eff}	crack size or depth of surface crack, effective value of a
c	half-length of surface crack
D_{r}, $D_{\text{r}}^{\max}$	applied strain parameter, limiting value of D_{r}
E	Young's modulus
E'	E in plane stress, $E/(1-\nu^2)$ in plane strain or axisymmetry
$f(L_{\text{r}})$	R6 failure assessment curve
$f^*(D_{\text{r}})$	strain-based failure assessment curve
F, F_{eff}	normalised K, value of F at a_{eff}
J	J-integral
J_{mat}	fracture resistance
K	stress intensity factor
K_{mat}	fracture toughness
K_{r}	R6 parameter
L_{r}, $L_{\text{r}}^{\max}$	R6 parameter, limiting value of L_{r}
n, N	exponents in stress–strain laws
P, P_{L}	load, limit load
t, w	plate thickness, half-plate width
T	temperature
x, y, z	Cartesian co-ordinates
α	constant in stress–strain law
δ	displacement
ε	strain
ε_0	normalising strain
$\bar{\varepsilon}$	equivalent strain
ε_{f}	strain at stress σ_{f}
ε_{y}	yield strain
ε_{Y}	elastic strain limit, σ_{Y}/E
λ	crack area fraction, $\pi ac/4tw$
ν	Poisson's ratio
ρ	R6 parameter
σ	stress
σ_0	normalising stress
$\bar{\sigma}$	equivalent stress
σ_{f}	flow stress, $(\sigma_{\text{u}}+\sigma_{\text{y}})/2$
σ_{u}	ultimate strength
σ_{y}	0.2% proof stress
σ_{Y}	limit of proportionality

Subscripts/superscripts

a	applied
c	cracked
el	elastic
i	ith component
max	maximum
nom	nominal
p	primary
pl	plastic
ref	reference

s	secondary
uc	uncracked

Abbreviations

ETM	engineering treatment model
FAD	failure assessment diagram
RSM	reference strain method
SB-FAD	strain-based failure assessment diagram

with R6 Option 2 but the various simplifying approximations within the RSM lead to quantitatively different results. Schwalbe [4] has also set down a strain-based approach for small cracks in plane stress, which has been incorporated within the GKSS engineering treatment model (ETM) [8]. The RSM and strain-based ETM are outlined in Section 3. The results of recent finite element (FE) calculations [9–12] for surface semi-elliptical defects in plates under mechanical and thermal loads are used in Section 4 to assess the RSM approximation. The strain-based *J*-estimation approach is then re-cast in Section 5 in terms of a strain-based FAD (SB-FAD).[1] A lower-bound curve on the SB-FAD is suggested for general application. Discussion and conclusions follow in Sections 6 and 7, respectively.

2. The R6 approach

The R6 [1] procedure requires the calculation of parameters L_r and K_r, dependent on load, geometry and material properties. For primary loading of magnitude P, L_r and K_r are defined by

$$L_r = P/P_L(a,\sigma_y) = \sigma_{ref}/\sigma_y \tag{1}$$

and

$$K_r = K/K_{mat} \tag{2}$$

where $P_L(a,\sigma_y)$ is the corresponding limit load for the component of crack size a and 0.2% proof stress σ_y, K is stress intensity factor, K_{mat} is fracture toughness and σ_{ref} is reference stress. Modifications to Eq. (2) are made for the case of secondary stresses [15]. Secondary stresses do not affect L_r. Welding residual stresses, in particular, can be primary or secondary, depending on the associated elastic follow-up. The assessment point (L_r, K_r) is then plotted on the FAD and compared with the failure assessment curve, $K_r = f(L_r)$, and the plastic collapse limit $L_r = L_r^{max} = \sigma_f/\sigma_y$, to assess proximity to the failure condition. Various 'Options' are set down in R6 for the function f. Failure is conceded when either $K_r = f(L_r)$, equivalent to $J = J_{mat}$ where J is the crack driving force parameter and $J_{mat} = K_{mat}^2/E'$ is the material's fracture resistance, or $L_r = L_r^{max}$. Here, $E' = E/(1-\nu^2)$, E and ν being Young's modulus and Poisson's ratio, respectively, and σ_f is flow stress, defined in R6 as the mean of σ_y and the material's ultimate strength, σ_u.

The loading parameters in Eqs. (1) and (2) are deduced in general from the uncracked-body elastic stresses in the plane of the defect. However, welding residual loads are often defined by bounding or more realistic stress distributions in compendia such as in R6. The resulting stress intensity factors then need to be derived. In this context, Dong and Hong [16] state that displacement-controlled boundary conditions may be more appropriate than stress-controlled for welding residual stresses.

It is known that, for displacement-controlled or strain-controlled loads, the basic R6 approach tends to be conservative, particularly for strains in excess of yield. Elastic calculation of the stresses (corresponding to the applied strains or displacements) in the plane of the defect tends to over-estimate the applied loads by neglecting compliance changes due to plasticity and/or the presence of the crack. Section III.14 of R6 provides an alternative, iterative approach that takes these effects into account [17]. Each constituent, δ_i, of a set of fixed applied displacements or rotations, δ, is written as

[1] It is noted that a SB-FAD approach has also been used to assess creep crack growth in creep-brittle steels [13,14].

$$\delta_i = \delta^{\mathrm{el}}_{i,\mathrm{uc}} + \delta^{\mathrm{pl}}_{i,\mathrm{uc}} + \delta^{\mathrm{el}}_{i,\mathrm{c}} + \delta^{\mathrm{pl}}_{i,\mathrm{c}} \tag{3}$$

where the subscripts 'uc' and 'c' denote 'uncracked' and 'cracked', respectively, and the superscripts 'el' and 'pl', denote 'elastic' and 'plastic'. The corresponding reaction loads or moments at the locations of the prescribed displacements are first estimated and then refined by iteration until the given boundary conditions are satisfied. The basic assessment route is then followed with $(L_\mathrm{r}, K_\mathrm{r})$ defined from the converged value of load. The simplest and most conservative approximation to Eq. (3) is to neglect all but the elastic uncracked-body displacements, $\delta^{\mathrm{el}}_{\mathrm{uc}}$. Addition of the uncracked-body plastic term, $\delta^{\mathrm{pl}}_{\mathrm{uc}}$ [3,5], and/or those reflecting the influence of the crack ($\delta^{\mathrm{el}}_{\mathrm{c}}$, $\delta^{\mathrm{pl}}_{\mathrm{c}}$) leads to successively less conservative estimates of the loading [17]. The most complex term in Eq. (3) to evaluate is, generally, $\delta^{\mathrm{pl}}_{\mathrm{c}}$.

3. Previous strain-based *J*-estimation methods

The reference strain method (RSM) [3] is based on the reference stress approximation to J [18] underlying R6, but re-written as

$$J = F^2 \pi a \sigma_{\mathrm{nom}} \varepsilon_{\mathrm{nom}} \left\{ \frac{\varepsilon_{\mathrm{ref}}/\sigma_{\mathrm{ref}}}{\varepsilon_{\mathrm{nom}}/\sigma_{\mathrm{nom}}} \right\} \tag{4}$$

where the stress intensity factor

$$K = F \sigma_{\mathrm{nom}} \sqrt{\pi a} \tag{5}$$

and σ_{nom}, $\varepsilon_{\mathrm{nom}}$ are the applied nominal stress and strain. The reference strain, $\varepsilon_{\mathrm{ref}}$, corresponds to the reference stress, σ_{ref}, on the stress–strain curve. It was noted that the term in brackets on the right hand side of Eq. (4) is equal to unity for elastic behaviour. Similarly, for small cracks and elastic–plastic material response, it is close to unity when $\sigma_{\mathrm{ref}}/\sigma_{\mathrm{nom}} \cong 1$, that is for essentially uniform tensile loading. Moreover, conservatism may result for bend loading, where $\sigma_{\mathrm{ref}} < \sigma_{\mathrm{nom}}$, and hence $\varepsilon_{\mathrm{ref}}/\sigma_{\mathrm{ref}} < \varepsilon_{\mathrm{nom}}/\sigma_{\mathrm{nom}}$, if σ_{nom} is taken as the elastic bending stress. For deeper cracks under tension loading, where $\sigma_{\mathrm{ref}}/\sigma_{\mathrm{nom}} > 1$, the bracketed terms exceed unity.

For small cracks in non-uniform stress and strain fields, Linkens et al. replace σ_{nom}, $\varepsilon_{\mathrm{nom}}$ in Eq. (4) by $\bar{\sigma}_{\mathrm{uc}}$, $\bar{\varepsilon}_{\mathrm{uc}}$ where the latter are the elastic–plastic uncracked-body equivalent stress and equivalent strain at the crack location. A factor of 2 is then applied to compensate for various simplifying approximations. This leads to, firstly,

$$J = 2F^2 \pi a \bar{\sigma}_{\mathrm{uc}} \bar{\varepsilon}_{\mathrm{uc}} \tag{6}$$

and then, bounding the applied stress by the flow stress, σ_f, to

$$J = 2F^2 \pi a \sigma_\mathrm{f} \bar{\varepsilon}_{\mathrm{uc}} \tag{7}$$

It was suggested that welding residual strains should be included by addition of the yield strain to the mechanical strain, $\bar{\varepsilon}_{\mathrm{uc}}$, in Eqs. (6) and (7). These equations were shown to be qualitatively similar to strain-based estimates of J due to earlier researchers albeit with differing numerical factors on the mechanical and yield strains. The precise definition of 'yield strain' is unclear but for practical applications will follow from the 0.2% and 1% plastic strain values recommended in R6 for ferritic and austentic steels, respectively.

A more accurate approximation, consistent with the small-scale yielding approximation to J in Option 2 of R6, was expressed [3] for small cracks in tension, where $\sigma_{\mathrm{ref}} \cong \bar{\sigma}_{\mathrm{uc}}$, as

$$J = F^2 \pi a \left(\bar{\sigma}_{\mathrm{uc}} \bar{\varepsilon}_{\mathrm{uc}} + \frac{\bar{\sigma}^5_{\mathrm{uc}}}{2E^2 \bar{\varepsilon}_{\mathrm{uc}} \sigma^2_\mathrm{y}} \right) \tag{8}$$

Schwalbe [4] also formulated a strain-based estimate of both J and crack-tip opening displacement in conditions of plane stress. The derivation was based on a symmetric crack of total length $2a$ in a plate of width $2w$ under tension loading, specifically a centre-cracked or double edge-notched plate. For stresses $\sigma > \sigma_\mathrm{Y}$, the material stress–strain relationship assumed was of the form $\varepsilon/\varepsilon_\mathrm{Y} = (\sigma/\sigma_\mathrm{Y})^{1/N}$ where $N < 1$, $\varepsilon_\mathrm{Y} = \sigma_\mathrm{Y}/E$ and σ_Y is the limit of proportionality. Then, for uniform tensile loading due to remote strain $\varepsilon_\mathrm{a} > \varepsilon_\mathrm{Y}$, setting the yield stress $\sigma_\mathrm{y} \cong \sigma_\mathrm{Y}/0.9$, the crack driving force, J, was given by

$$J = 0.81\sigma_Y^{1-N}(1-a/w)^2E^N\pi aF_{\text{eff}}^2(1+0.405(1-a/w)^2F^2)\varepsilon_a^{1+N} \tag{9}$$

and

$$J = 1.14\pi a\sigma_Y(E/\sigma_Y)^N\varepsilon_a^{1+N} \tag{10}$$

for the finite width and infinitely wide plates ($a/w \to 0$), respectively. Here F_{eff} denotes $F(a_{\text{eff}})$ where $a_{\text{eff}} = a + (K/\sigma_Y)^2/2\pi$ and F, F_{eff} are evaluated at stress σ_Y. For $a/w \to 0$, F, $F_{\text{eff}} \to 1$. Eqs. (9) and (10) were shown to agree well with experimental and finite element data for 3 aluminium and steel centre-cracked plate specimens. The applied strain, ε_a, was identified with the gauge length strain for short cracks.

Eq. (10) can be simply compared[2] with Eq. (7) for small cracks when $\varepsilon_a \cong \bar{\varepsilon}_{uc}$ and $F \cong 1$:

$$\frac{J(\text{Eq. (10)})}{J(\text{Eq. (7)})} = \frac{1.14\pi a\sigma_Y^{1-N}E^N\varepsilon_a^{1+N}}{2\pi a\sigma_f\varepsilon_a} = \frac{0.57(E\varepsilon_a/\sigma_Y)^N}{\sigma_f/\sigma_Y} \tag{11}$$

The right hand side of Eq. (11) depends on strain level and material properties, being greater than unity for very high strain levels but less than unity for moderate strain levels where $(E\varepsilon_a/\sigma_Y)^N \cong \sigma_f/\sigma_y$, that is for stresses corresponding to those at the flow stress.

4. Finite element analysis

Finite element (FE) J results have been reported by Lei [9–11] for a semi-elliptical surface crack of depth a and length $2c$ in a plate of thickness t and width $2w$ under tension, bending and combined bending and tension. Additional results were reported [12] for the case of tension plus a temperature field varying across the width of the plate. The mechanical loads were applied under load control. The cases considered here are listed in Tables 1 and 2. Only the deepest point of the crack is considered. Table 1 includes the cracked area fraction of the plate cross-section, $\lambda = \pi ac/4tw$. The remote stress distribution is uniaxial so that the remote strain components and hence equivalent strain, $\bar{\varepsilon}_a = \bar{\varepsilon}_{uc}$, may be simply determined. Although the stress and strain fields in the cracked plate vary away from its loaded ends, for small area fractions ($\lambda \ll 1$), the remote strain normal to the crack plane may be approximately related to the plate elongation. The values of λ in Table 1 are all less than 0.1. The FE results showed that the effect of the crack on the specimen compliance is negligible. For the present purposes, the variation of J with either remote strain or displacement can then be plotted. This avoids the need to re-run the analyses under displacement control. The factor F in Tables 1 and 2 is the normalised stress intensity factor as given by Eq. (5), with σ_{nom} taken as the remote tension or bending stress, as appropriate.

4.1. Mechanical loading

The material's stress–strain law was of Ramberg–Osgood type:

$$\frac{\varepsilon}{\varepsilon_0} = \frac{\sigma}{\sigma_0} + \alpha\left(\frac{\sigma}{\sigma_0}\right)^n \tag{12}$$

where $n > 1$, $\sigma_0 = 1$ MPa, $\varepsilon_0 = \sigma_0/E$, $E = 500$ MPa and $\alpha = 1$, so that σ_0 equals the 0.2% proof stress, σ_y. Figs. 1–4 plot various estimates of normalised J, $J/(\sigma_0 a)$, against applied strain ratio, $\bar{\varepsilon}_a/\varepsilon_0$, at the deepest point of the crack, for the case of tension loading with $n = 5$. Several curves are plotted. These include curves labelled 'Opt 2 (strain)' and 'Opt 2 (stress)'. In the former, the remote stress, σ_a, perpendicular to the crack plane which corresponds to the given equivalent strain ratio, $\bar{\varepsilon}_a/\varepsilon_0$, is evaluated from Eq. (12). The stress is then converted into a reference stress [19] and J evaluated using R6 Option 2. The upper line in the Figures, marked 'Opt 2 (stress)', shows the result if the remote stress is calculated on an elastic basis, that is $\sigma_a = E\bar{\varepsilon}_a$. The lower line in the Figures is then equivalent to including the first two terms on the right hand side of Eq. (3) whereas the upper line uses only the first term. The expressions of Eqs. (6) and (7) are also plotted and labelled as 'Linkens

[2] The RSM uses applied equivalent strain to evaluate J. The strain in the ETM is not clearly defined but equating it with the gauge length strain suggests component strain. In Eq. (11), the differences are neglected.

Table 1
Normalised stress intensity factor and crack area ratio for a semi-elliptical crack in a plate under tension or bending

w (mm)	c (mm)	a/t	a/c	F [22][a]	λ
Tension					
120	30	0.2	0.2	1.1309	0.0393
120	30	0.2	0.6	0.8671	0.0393
120	30	0.5	0.2	1.4518	0.0982
120	30	0.5	0.6	0.9588	0.0982
Bending					
120	30	0.2	0.6	0.6449	0.0393

[a] At deepest point of crack.

Table 2
Maximum temperature and secondary stress intensity factor for a semi-elliptical crack in a plate under tension and thermal load

w (mm)	c (mm)	a/t	a/c	T_{max} (°C)	K^s (MPa mm$^{0.5}$)[a] [12]
120	30	0.2	0.2	500	10.732
120	30	0.5	0.6	500	15.429

[a] At deepest point of crack.

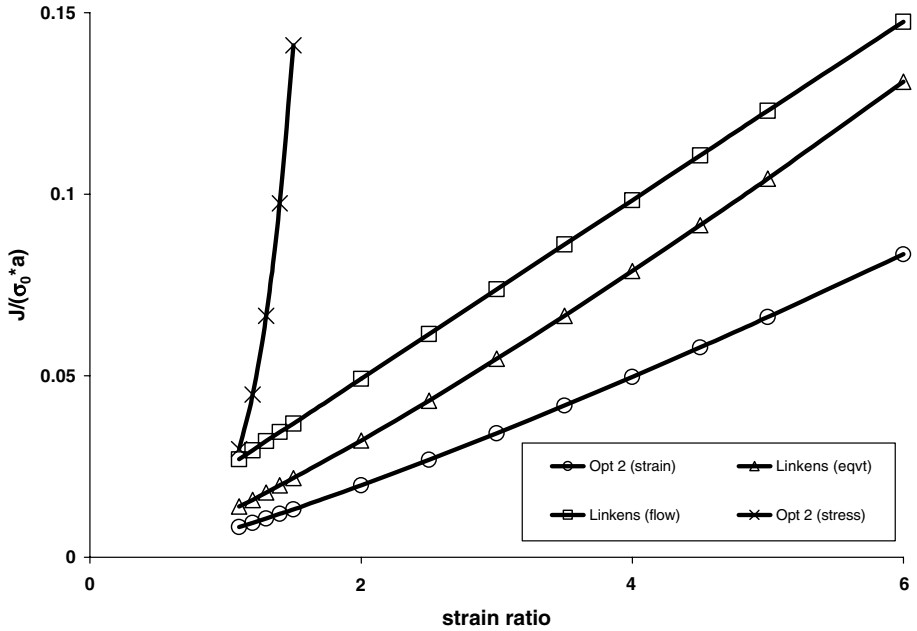

Fig. 1. Plot of normalised J against applied strain ratio for $a/t = a/c = 0.2$; tension load.

(eqvt)' and 'Linkens (flow)', respectively. The flow stress is taken as $\sigma_f = 1.53\sigma_0$, using a correlation of $1/n$ with σ_u/σ_y [1].

The global reference stress equation [19] led to close estimates of the FE J values using R6 Option 2 [9]. The actual FE values of J are therefore not shown as they are close to those predicted by the 'Opt 2 (strain)' curve. It can be seen that, as expected, the elastic, stress-based route ('Opt 2 (stress)') significantly over-estimates J for strains in excess of the yield strain, ε_0. It can also be seen that the RSM approximations are closer to but in

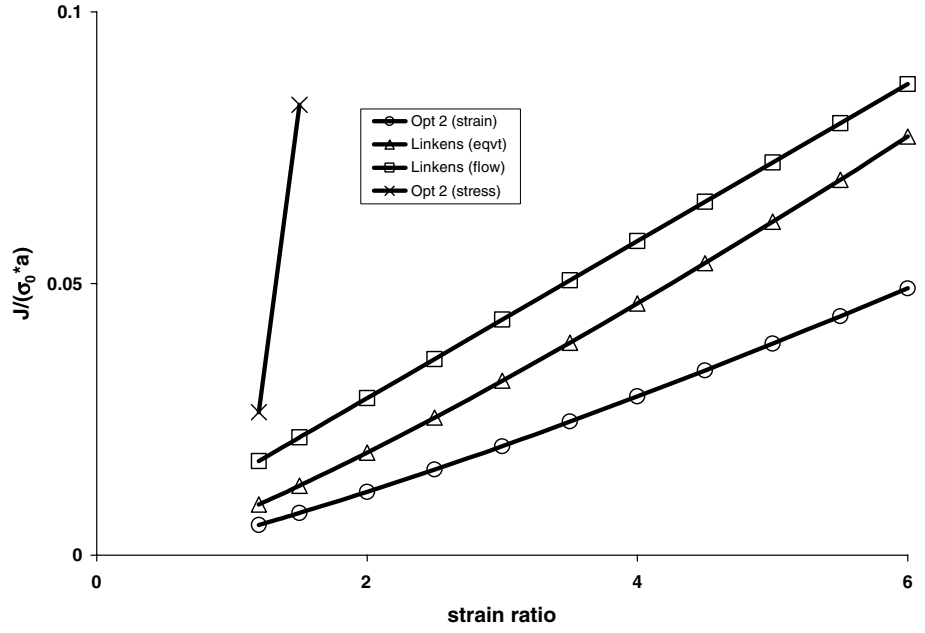

Fig. 2. Plot of normalised J against applied strain ratio for $a/t = 0.2$, $a/c = 0.6$; tension load.

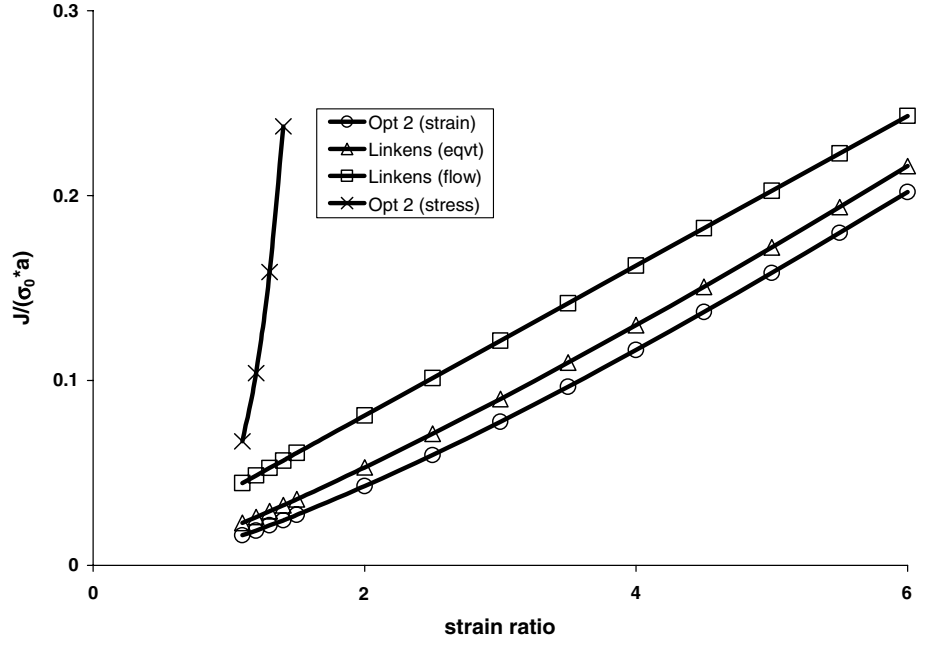

Fig. 3. Plot of normalised J against applied strain ratio for $a/t = 0.5$, $a/c = 0.2$; tension load.

excess of the 'Opt 2 (strain)' curve. The strain-based estimates of Eqs. (6) and (7) tend to approach the 'Opt 2 (strain)' curve as the crack becomes deeper. This is expected as the approximate relationships use uncracked-body stresses and may therefore under-estimate J for deep cracks.

Fig. 5 show similar results for $J/(\sigma_0 a)$ against strain ratio, $\bar{\varepsilon}_a/\varepsilon_0$, at the deepest point of the crack for bend load in the particular case $a/t = 0.2$, $a/c = 0.6$ and $n = 5$. The component and hence equivalent strain at the

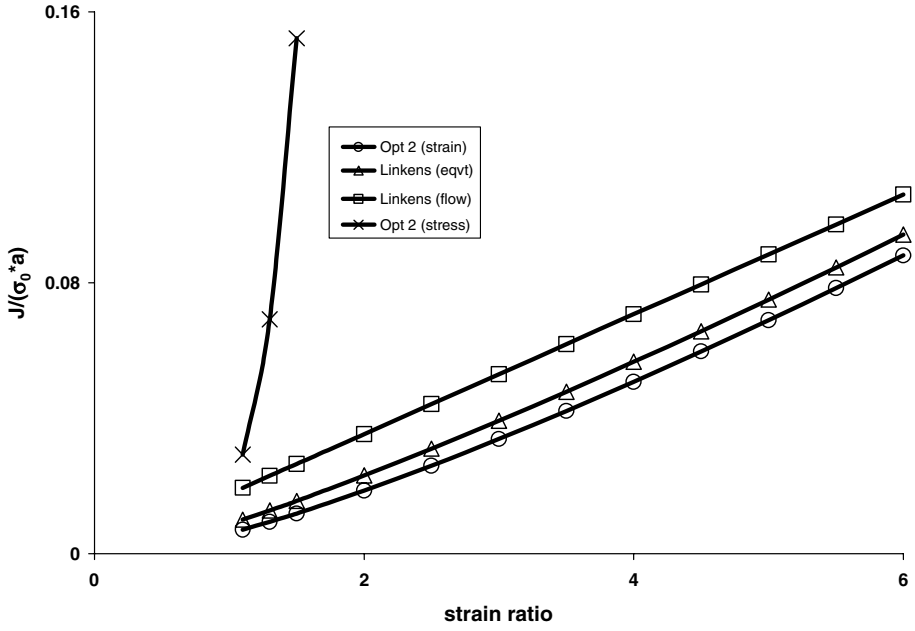

Fig. 4. Plot of normalised J against applied strain ratio for $a/t = 0.5$, $a/c = 0.6$; tension load.

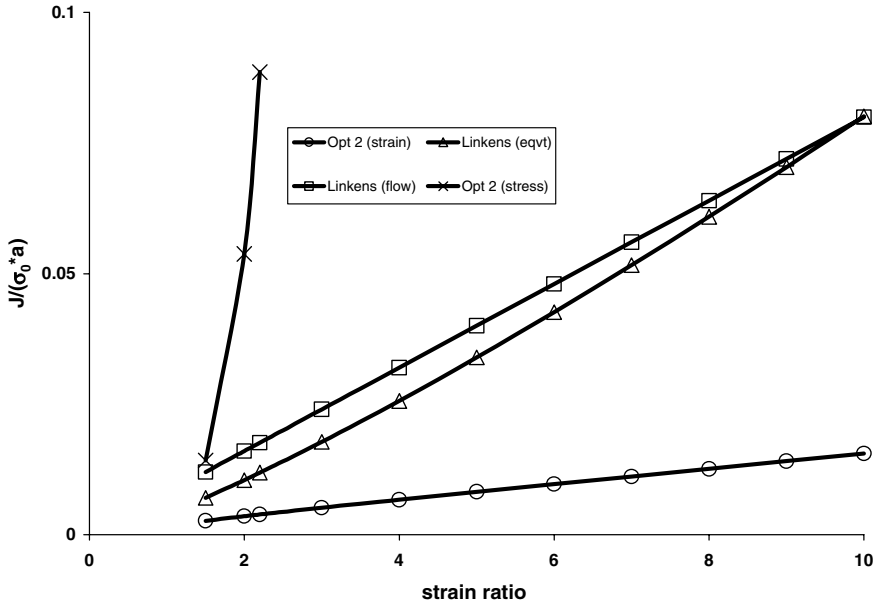

Fig. 5. Plot of normalised J against applied strain ratio for $a/t = 0.2$, $a/c = 0.6$; bending load.

cracked surface, corresponding to the applied uniaxial stress, may be simply calculated. The appropriate F for the bending stress distribution is included. Similarly, the R6 Option 2 estimates are based on the Goodall and Webster [19] bending equation when calculating σ_{ref}. The stress-based route conservatively over-estimates the FE J values as for the case of tension loading. It can be seen that the conservatism of the RSM for bend load is greater than that for tension load (compare Figs. 1 and 2 with Fig. 5). It should be noted that the RSM estimates use the surface value of stress and strain rather than, say, those at a distance into the plate equal to the crack depth.

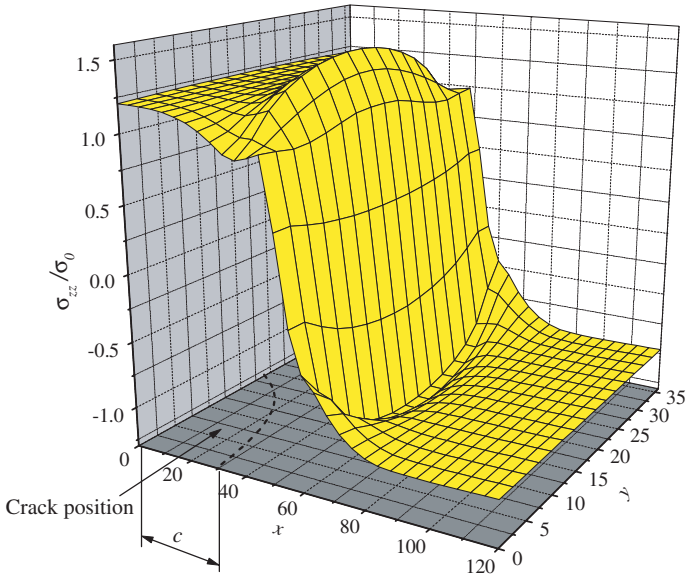

Fig. 6. Variation of stress, normal to the plane of the prospective crack, in the uncracked plate; thermal load only, elastic–plastic properties.

4.2. Thermal and mechanical loading

The stress–strain law [12] is $\varepsilon/\varepsilon_0 = (\sigma/\sigma_0)^5$ for $\sigma > \sigma_0$ with $\sigma_0 = 1$ MPa and $E = \sigma_0/\varepsilon_0 = 500$ MPa, such that the 0.2% and 1% proof stresses are $\sigma_y = 1.167\sigma_0$ and $1.452\sigma_0$, respectively. The corresponding total strains at these stresses are 0.0043 and 0.0129. An applied temperature field, $T(x)$, varies symmetrically across the width of the plate, with $T = 0$ at the centre of the plate ($x = 0$) and $T(x) = T_{\max}$ for $x/w \geqslant 0.5$. The maximum temperature $T_{\max} = 500$ °C, the most severe of the cases studied by Lei [12]. Note that the temperature does not vary in the direction of the crack depth. The cases considered here are listed in Table 2. The elastic–plastic thermal stress normal to the plane of the prospective crack is shown in Fig. 6. Note that the stress across the middle of the plate is tensile and in excess of the 0.2% proof stress, balanced by yield magnitude compression near the plate sides, representative of certain welding residual stress distributions.

The R6 estimate of J under combined primary and secondary stress [15] is

$$J^{\mathrm{p+s}} = J^{\mathrm{p}}\left(\frac{f}{f-\rho}\right)^2\left(1+\frac{K^{\mathrm{s}}}{K^{\mathrm{p}}}\right)^2 \tag{13}$$

where the superscripts p and s denote primary and secondary, respectively, and ρ is the R6 correction factor for combined stresses. Since $\rho \leqslant 0$ for $L_r \geqslant 1$, approximately, and noting that $J^{\mathrm{p+s}} \geqslant J^{\mathrm{p}} + J^{\mathrm{s}}$ [15], it follows from Eq. (13) that, for $L_r \geqslant 1$,

$$J^{\mathrm{p}} + J^{\mathrm{s}} \leqslant J^{\mathrm{p+s}} \leqslant \left(1+\frac{K^{\mathrm{s}}}{K^{\mathrm{p}}}\right)^2 J^{\mathrm{p}} \tag{14}$$

Note that the right hand side of Eq. (14) becomes $(1 + \sigma^{\mathrm{s}}/\sigma^{\mathrm{p}})^2 J^{\mathrm{p}}$ in the case of load-controlled membrane approximations to the primary (σ^{p}) and secondary (σ^{s}) stress. Estimates of J under combined stresses have been formulated by other authors [20,21] and differ in detail from the R6 approach. The RSM [3] estimate of J for combined mechanical and residual stresses, Eq. (7), taking the thermal stress as equivalent to a welding residual stress, corresponds to $J \cong J^{\mathrm{p}}(1 + \varepsilon_y/\bar{\varepsilon}_a)$, where ε_y is the representative yield strain.

The FE results [12] may be compared with the RSM approximations and with the upper bound of Eq. (14), with ε_y equal to the total strain of 0.0129 at the 1% proof stress, representative of an austenitic steel [1]. Figs. 7 and 8 show some results as $J/(\sigma_0 a)$ against applied mechanical strain ratio, $\bar{\varepsilon}_a/\varepsilon_0$. Then $J \neq 0$ at $\bar{\varepsilon}_a/\varepsilon_0 = 0$ due

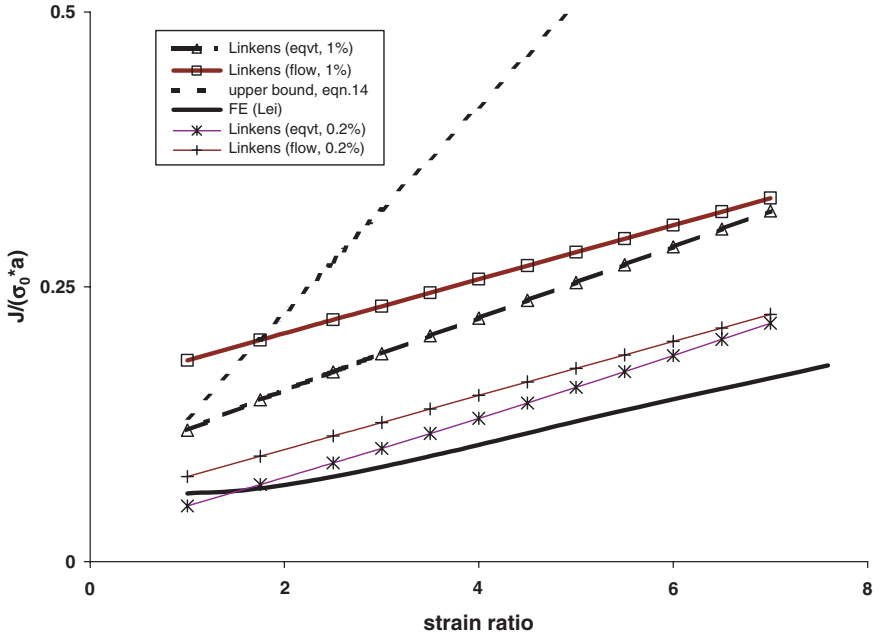

Fig. 7. Plot of normalised J against applied mechanical strain ratio for $a/t = 0.2$, $a/c = 0.2$; tension + thermal load.

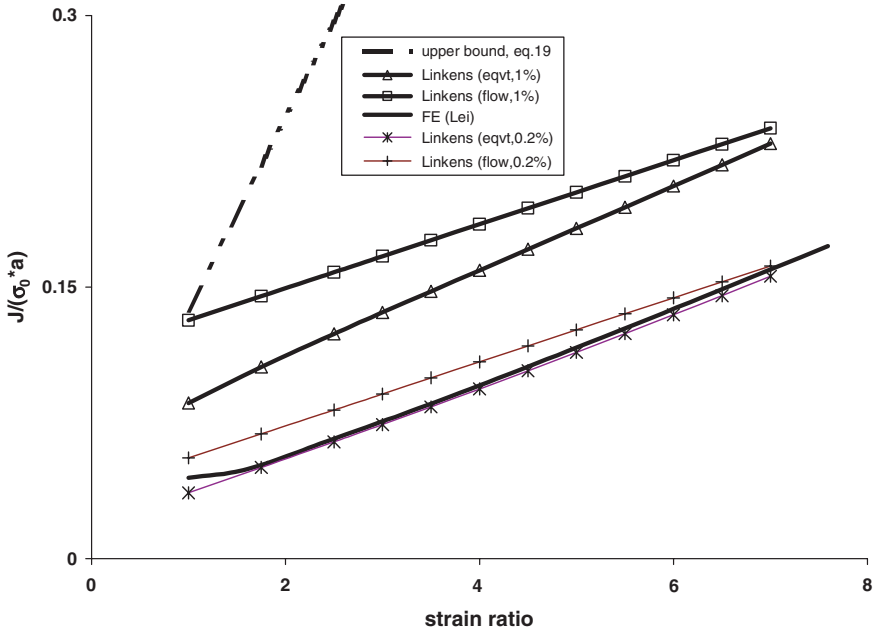

Fig. 8. Plot of normalised J against applied mechanical strain ratio for $a/t = 0.5$, $a/c = 0.6$; tension + thermal load.

to the thermal stress acting alone. The R6 Option 2 estimate of J^p is obtained as in Section 4.1. It can be seen that all the estimates are very conservative compared with the FE results. The use of a total strain of 0.0043 corresponding to 0.2% plastic strain, instead of 0.0129, reduces the overall level of conservatism as can also be seen in Figs. 7 and 8. The close agreement with the FE results in this latter case should be contrasted with the corresponding overestimation in Figs. 1 and 4 for pure mechanical load.

5. The strain-based failure assessment diagram

A strain-based approach can be founded either on a reference stress (and hence L_r) deduced from the geometry and applied strain or displacement via the material's stress–strain curve [5,17] or directly within a strain-based FAD (SB-FAD) formulation. The former has the advantage of retaining the conventional L_r-based FAD but loses its simple graphical interpretation in terms of margin on applied load. The alternative SB-FAD approach is considered in this section.

Define the axes of the SB-FAD as D_r and K_r. The abscissa, D_r, is given by

$$D_r = \varepsilon_{ref}/\varepsilon_y \tag{15}$$

where $\varepsilon_y = \sigma_y/E$ and the reference strain, ε_{ref}, remains to be defined. Then, from Eqs. (1) and (15)

$$D_r = L_r(E\varepsilon_{ref}/\sigma_{ref}) \tag{16}$$

where $(\varepsilon_{ref}, \sigma_{ref})$ lies on the stress–strain curve. The reference strain, ε_{ref}, should reduce to $\varepsilon_{ref} = \sigma_{ref}/E$, so that $D_r/L_r \to 1$, in the elastic limit. The ordinate, K_r, follows from Eq. (2) with K evaluated at the load level corresponding to σ_{ref}.

A strain-based collapse limit on D_r, consistent with the usual stress-based limit of $L_r^{max} = \sigma_f/\sigma_u$, is then [3]

$$D_r^{max} = \varepsilon_f/\varepsilon_y \tag{17}$$

where $\varepsilon_f = \varepsilon(\sigma_f)$ is the uniaxial strain at the flow stress from the true stress–true strain curve. It may be argued that plastic collapse would not occur under strain control until significant plastic strain levels at which ε_{ref} is comparable with the material's true uniform elongation [5]. The collapse limit of Eq. (17) introduces a degree of additional conservatism.

Eqs. (2), (15) and (17), together with a suitable definition of the shape of the failure assessment curve $K_r = f^*(D_r)$ define the SB-FAD approach. The function f^* is defined following R6 Option 3 [1] by the variation with D_r of

$$f^*(D_r) = (J^{el}/J)^{0.5} \tag{18}$$

The remainder of this section addresses the determination of f^* and ε_{ref}.

5.1. Strain-based failure assessment curves based on the RSM

For the shallow crack under predominantly tension loading, where $(\varepsilon_{ref}, \sigma_{ref}) \cong (\bar{\varepsilon}_{uc}, \bar{\sigma}_{uc})$ and the stress $\bar{\sigma}_{uc}$ follows from the stress–strain law at a strain of $\bar{\varepsilon}_{uc} = D_r\varepsilon_y$, the RSM [3] approximations to J in Eqs. (7) and (8), together with $J^{el} = K^2/E$, lead[3] to

$$f^*(D_r) = \left(\frac{\bar{\sigma}_{uc}^2}{2E\sigma_f\bar{\varepsilon}_{uc}}\right)^{0.5} = \left(\frac{\bar{\sigma}_{uc}^2}{2ED_r\varepsilon_y\sigma_f}\right)^{0.5} \tag{19}$$

and

$$f^*(D_r) = \left(\frac{E\bar{\varepsilon}_{uc}}{\bar{\sigma}_{uc}} + \frac{\bar{\sigma}_{uc}^3}{2E\bar{\varepsilon}_{uc}\sigma_y^2}\right)^{-0.5} = \left(\frac{ED_r\varepsilon_y}{\bar{\sigma}_{uc}} + \frac{\bar{\sigma}_{uc}^3}{2E^3D_r\varepsilon_y^3}\right)^{-0.5} \tag{20}$$

respectively.

Note that $f^* \to 1$ from Eq. (20) as $D_r \to 0$ $(E\bar{\varepsilon}_{uc}/\bar{\sigma}_{uc} \to 1)$. However, from Eq. (19), $f^* \to 2^{-0.5}(\bar{\sigma}_{uc}/\sigma_f)^{0.5} < 1$ as $D_r \to 0$. The latter limit simply reflects the conservatism implicit in Eq. (7) following from both setting $\bar{\sigma}_{uc} = \sigma_f$ and incorporating the additional factor of 2 on J. Eq. (19) should be restricted to $D_r > 1$; for $D_r < 1$, the bound $\bar{\sigma}_{uc} < \sigma_f$ is overly conservative.

Eqs. (15), (17) and (19) or (20) provide the basis of Option 2 failure assessment curves within a SB-FAD approach. The restriction is that the size of the crack should be sufficiently small such that the compliance

[3] Making the usual assumption that $E' \cong E$.

of the structure is not significantly affected. This is consistent with Bratfos [5], where the loads corresponding to applied bending strains and tension forces on pipelines are deduced from uncracked-body analysis. Bratfos also remarks that, within an Option 2 approach, the same stress–strain curve should be used to construct the failure assessment curve as used to calculate the reference stress. The defect is accounted for in the definition of σ_{ref}. For deep cracks, further work is required to quantify ε_{ref} in terms of the applied strains, consistent with the approach [17] of R6 Section III.14 as outlined earlier. It is noted only that the load, P, corresponding to the applied displacements or rotations leads to σ_{ref} and hence ε_{ref} and D_{r}. The derived values are conservative when the cracked-body contribution is neglected.

5.2. Approximate strain-based failure assessment curves

The R6 Option 1 failure assessment curve was derived as an approximate lower bound to Option 2 curves for a range of austenitic and ferritic materials. A logical development of strain-based Option 2 curves, such as Eqs. (19) and (20), would be the derivation of an equivalent lower bound in (D_{r}, K_{r}) space. The Option 1 and Approximate Option 2 approaches [1] are used here as the starting point towards a generic curve. Defining the FAD in (L_{r}, K_{r}) space then requires only σ_{y} and σ_{u} in the case of a material with continuous yield point behaviour.

From the R6 Option 2 reference stress approximation to J, see Eq. (8), and the definition of the failure assessment curve, $K_{\text{r}} = f(L_{\text{r}}) = \sqrt{J^{\text{el}}/J}$, D_{r} and L_{r} are related by

$$D_{\text{r}} = \frac{L_{\text{r}}}{2f^2(L_{\text{r}})}\left(1 + \sqrt{1 - 2L_{\text{r}}^2 f^4(L_{\text{r}})}\right) \tag{21}$$

Hence the R6 Option 1 curve,

$$f(L_{\text{r}}) = (1 + 0.5L_{\text{r}}^2)^{-1/2}(0.3 + 0.7\exp(-0.6L_{\text{r}}^6)) \tag{22}$$

an explicit function of L_{r}, leads to an equivalent general curve in (D_{r}, K_{r}) space. This curve is shown in Fig. 9. At low $D_{\text{r}}(D_{\text{r}} < 1)$, $f^*(D_{\text{r}})$ is close to $(1 + 0.5D_{\text{r}}^2)^{-1/2}$ as also seen from Fig. 9. At higher D_{r}, a similar correction to that used to define $f(L_{\text{r}})$ in Eq. (22) could be developed to give a simple algebraic expression for $f^*(D_{\text{r}})$.

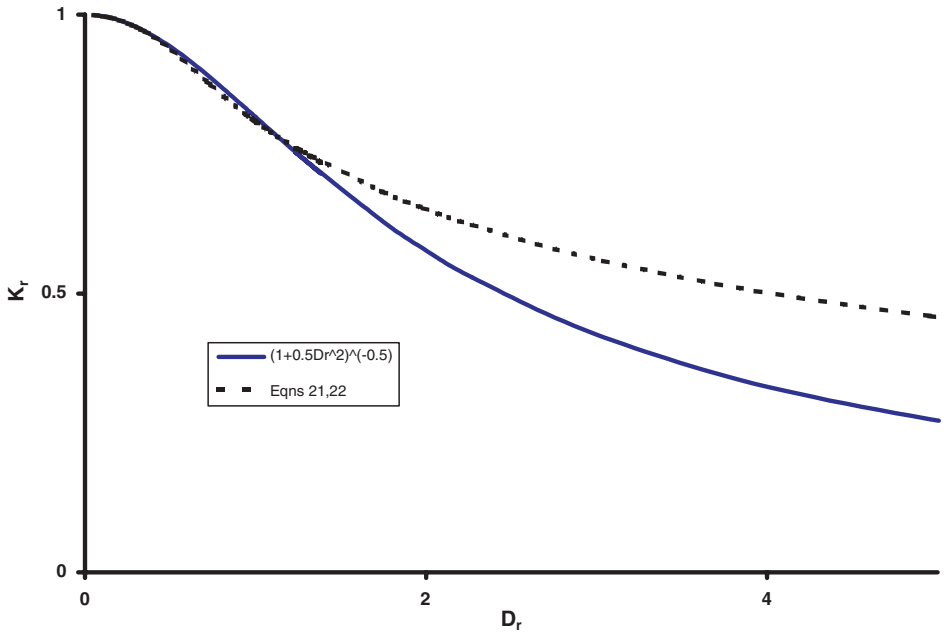

Fig. 9. Comparison of the strain-based failure assessment curve defined by Eqs. (21) and (22) with the approximation for small D_{r}.

For the R6 Approximate Option 2 route, the failure assessment curve in the plastic range, $L_r > 1$, is given [1] in the form $f(L_r) = f(1)L_r^{(N-1)/2N}$ where $0 < N = 0.3(1 - \sigma_y/\sigma_u) < 0.3$. The constant of proportionality, $f(1)$, depends on E/σ_y [1]. Neglecting the first-order plasticity correction for $L_r > 1$, that is setting $J/J^{el} \cong E\varepsilon_{ref}/\sigma_{ref} = D_r/L_r$, the SB-FAD is approximately defined from $K_r = f^*(D_r) = f(L_r)$ where $D_r = L_r/f^2(L_r)$. This fixes the plastic portion of the failure assessment curve as

$$f^*(D_r) = f^*(1)D_r^{(N-1)/2}, \quad D_r \geqslant 1/f^2(1) > 1 \tag{23}$$

with $f^*(1) = f(1)^N$. For $L_r < 1$, the approximate curve $f^*(D_r) = (1 + 0.5D_r^2)^{-1/2}$ is adopted and hence $f^*(1) = 0.816$ is fixed, independent of N. This Approximate Option 2 curve can be plotted on the SB-FAD.

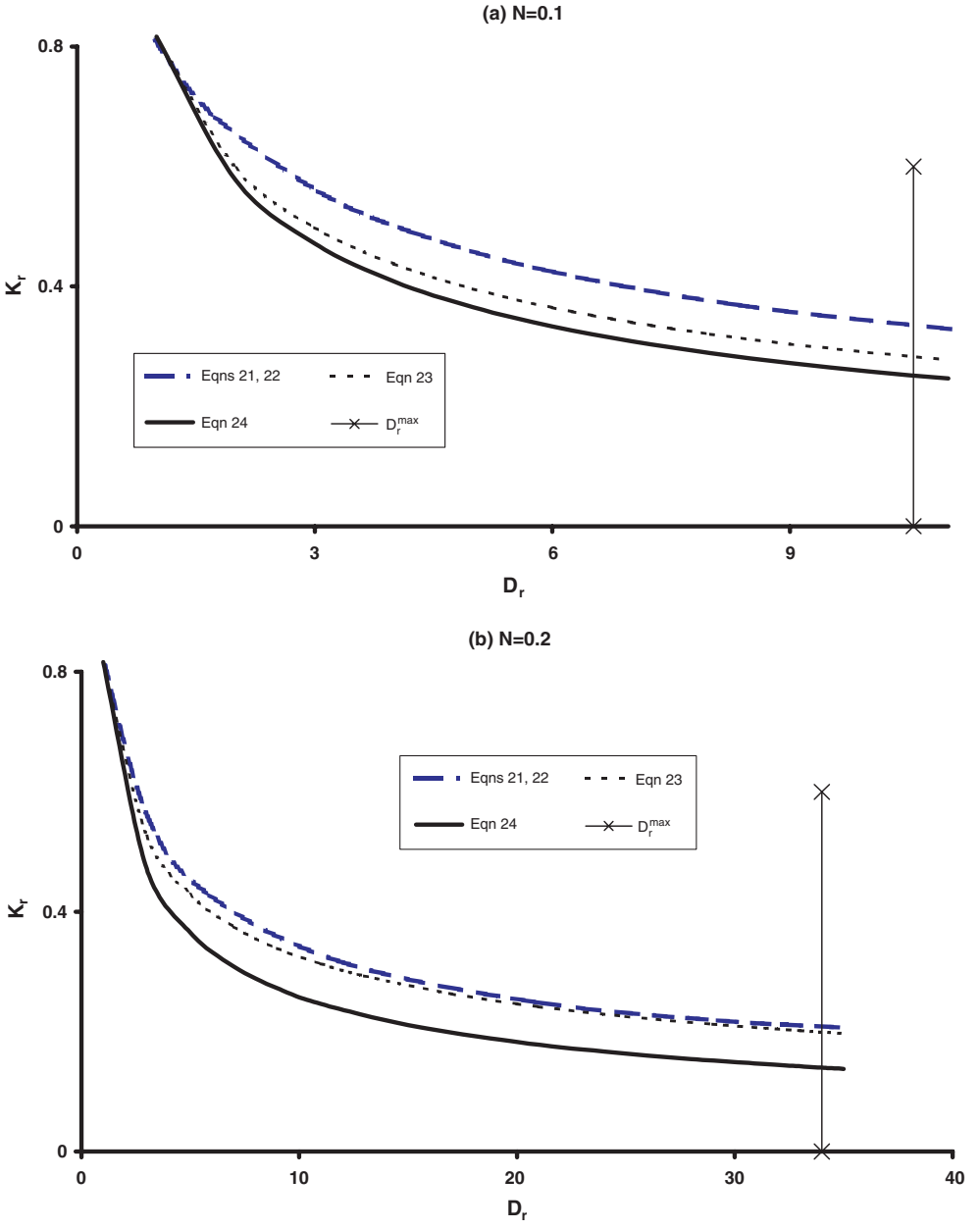

Fig. 10. Comparison of Approximate Option 2 strain-based failure assessment curves for $N = 0.1$ and $N = 0.2$ with Eqs. (21) and (22) and with the Option 1 curve of Eq. (24).

Examples, for $N = 0.1$ and $N = 0.2$, are shown in Fig. 10, which includes the appropriate values of the cut-off, D_r^{max}. The curve expressed by Eqs. (21) and (22), for $D_r > 1$, is also plotted.

Then setting $N = 0$ in Eq. (23), the curve $f^* \propto D_r^{-1/2}$, corresponding to an elastic-perfectly plastic stress–strain material, forms a lower bound to the failure assessment curve when $D_r > 1$; see Fig. 10. As noted above, $f^*(1) = 0.816$ is estimated from the first order plasticity correction $(1 + 0.5D_r^2)^{-1/2}$ at $D_r = 1$. This leads to the general curve

$$\begin{aligned} f^* &= (1 + 0.5D_r^2)^{-0.5}, \quad D_r \leqslant 1 \\ f^* &= f^*(1)D_r^{-1/2}, \quad D_r > 1 \end{aligned} \tag{24}$$

It can be seen that a hierarchy of failure assessment curves has been defined, consistent with the range of Options in R6. Validation is considered in the following section.

6. Discussion

The comparisons of the RSM and R6 Option 2 estimates of J suggest that the RSM conservatively predicts J at the deepest point of the crack for some simple three-dimensional components where the crack occupies a low to moderate fraction of the plate cross-section. The conservatism reduces for larger cracks and is likely that the RSM will be non-conservative for larger cracks. This is consistent with the conclusions of Linkens et al. [3]. The assumptions in the derivation of the ETM [4,8] leading to Eqs. (9) and (10) are more restrictive than those underlying the RSM expressions of Eqs. (6) and (7). However, the simple comparison of Eq. (11) suggests that the ETM leads to lower values of J for practicable strain ranges. Detailed comparisons of the ETM and RSM have not been performed here.

The alternative, SB-FAD approach to strain-based assessment is relatively simple to use and, for small defects, may be summarised as follows. It is similar to the conventional stress-based FAD approach.

(i) Define $D_r = \bar{\varepsilon}_{uc}/\varepsilon_y$.
(ii) Define $\bar{\sigma}_{uc}$ as the point on the stress–strain curve at strain $\bar{\varepsilon}_{uc}$.
(iii) Define $K_r = F\bar{\sigma}_{uc}\sqrt{\pi a}/K_{mat}$.

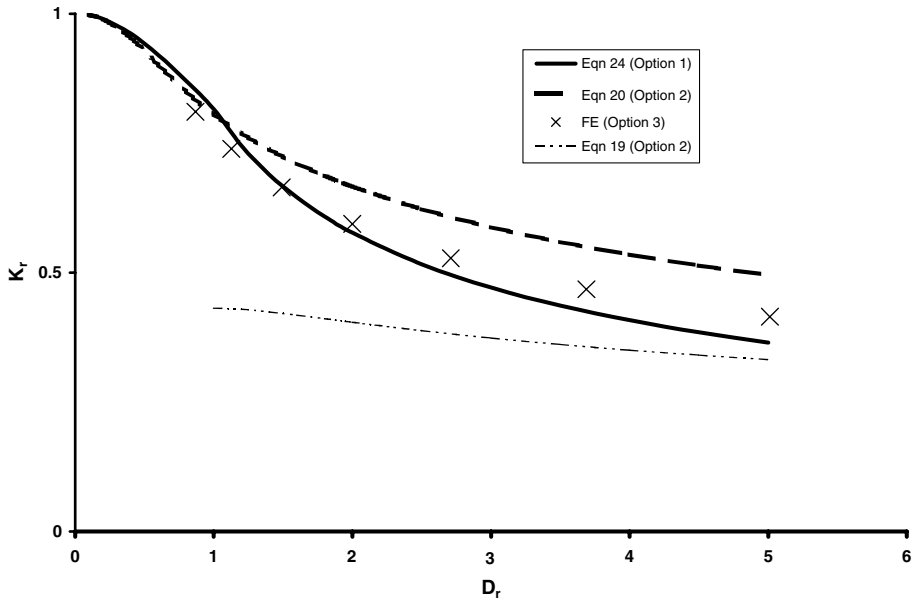

Fig. 11. Comparison of the Option 1, Option 2 and Option 3 strain-based failure assessment diagrams for the plate with $a/t = a/c = 0.2$ under tension load.

(iv) Define the failure assessment curve $f^*(D_r)$.
- Option 1—a simple approximation such as Eq. (24).
- Option 2—by Eq. (19) or Eq. (20).
- Approximate Option 2—using Eq. (23).
- Option 3—from FE analysis via Eq. (18).

(v) Define the cut-off, D_r^{max}, on the SB-FAD using Eq. (17).

(vi) Plot the point (D_r, K_r) on the SB-FAD defined by steps (iv) and (v). If the point is within the SB-FAD then failure is avoided.

The results of applying this approach to the plate with $a/t = a/c = 0.2$ and $n = 5$, assessed in Section 4.1, are shown in Fig. 11. For plotting the FE data, K_{mat} is taken as $(E'J_{FE})^{1/2}$ where J_{FE} is the FE value of J. The FE points lie close to but outside the Option 1 SB-FAD for $D_r > 1.5$, which is conservative. The Option 2 curve of Eq. (20) is outside the FE data, consistent with Eq. (20) underestimating the FE values of J. This implies that Eq. (20) should be used with caution when defining the SB-FAD. However, Eq. (19) is conservative, corresponding to its overestimation of J in Figs. 1–4.

It is judged that the SB-FAD approach requires further consideration prior to inclusion in failure assessment procedures such as R6, particularly with respect to the definition of ε_{ref} for larger cracks, and additional FE validation is required. Also, for general use, its application on welded structures with significant strength mis-match needs to be elucidated [5].

7. Conclusions

Strain-based approaches to fracture assessment have been considered. Recent published work has been contrasted with the alternative approach in R6 for fixed displacement loads. The derivation of an approximate strain-based FAD (SB-FAD) approach to fracture assessment has then been described. The following conclusions have been obtained.

(1) Finite element calculations show that the simplified approximate J expressions of Linkens et al. conservatively over-estimate J for semi-elliptical cracks in plates under tension. The conservatism reduces for deeper cracks.
(2) For bend loading, the simplified formulae of Linkens et al. also conservatively over-estimate J. The conservatism is greater than that for tensile loading due to the neglect of the through-wall stress gradient.
(3) Strain-based estimates of crack driving force, J, have been recast in the form of a strain-based FAD. A range of simple, approximate failure assessment curves and a SB-FAD assessment procedure have been described.
(4) Further work is required to generalise and validate the SB-FAD approach and to refine the limits of applicability prior to developing explicit recommendations for incorporation in fitness-for-service procedures such as R6.

Acknowledgments

This paper is published by permission of British Energy Generation Ltd. The assistance of Dr. Y. Lei in making available the detailed results of his finite element analyses is also gratefully acknowledged.

References

[1] R6. Assessment of the integrity of structures containing defects. Revision 4, Amendment 4, British Energy, Gloucester, 2005.
[2] BS7910:1999. Guide on methods for assessing the acceptability of flaws in metallic structures, incorporating Amendment 1. British Standards Institution, London, 2000.
[3] Linkens D, Formby CL, Ainsworth RA. A strain-based approach to fracture assessment—example applications. In: Proceedings of the conference engineering structural integrity assessment, Cambridge, EMAS, 2000.

[4] Schwalbe K-H. The crack tip opening displacement and *J* integral under strain control and fully plastic conditions estimated by the engineering treatment model for plane stress tension. ASTM STP, 1207. Philadelphia: ASTM; 1994. p. 636–51.
[5] Bratfos HA. Use of strain-based ECA for the assessment of flaws in pipeline girth welds subjected to plastic deformations. In: Proceedings of the international conference, high-grade linepipes in hostile environments, Yokohama, 7–8 November 2002. Scientific Surveys Ltd., Beaconsfield. p. 957–85, ISBN 0-901360-31-7.
[6] Wang Y-Y, Rudland D, Denys R, Horsley D. A preliminary strain-based design criterion for pipeline girth welds. Proceedings of the IPC'02, 4th international pipeline conference, Calgary, September 29–October 3, 2002. New York: ASME; 2002.
[7] Østby E, Jayadevan KR, Thaulow C. Fracture response of pipelines subject to large plastic deformation under bending. Int J Pressure Vessels Piping 2005;82:201–15.
[8] Schwalbe K-H, Zerbst U. The engineering treatment model. Int J Pressure Vessels Piping 2000;77:905–18.
[9] Lei Y. *J*-integral and limit load analysis of semi-elliptical surface cracks in plates under tension. Int J Pressure Vessels Piping 2004;81:21–30.
[10] Lei Y. *J*-integral and limit load analysis of semi-elliptical surface cracks in plates under bending. Int J Pressure Vessels Piping 2004;81:31–41.
[11] Lei Y. *J*-integral and limit load analysis of semi-elliptical surface cracks in plates under combined tension and bending. Int J Pressure Vessels Piping 2004;81:43–56.
[12] Lei Y. A comparison of 3-D finite element and simplified estimates of *J* under thermal and mechanical loads. ASME PVP, vol. 437, 2002.
[13] Smith DJ, Fookes AJ, Lamb M, Dean DW. Development of a strain-based FAD for prediction of creep cracking in welds. In: Proceedings of the international conference on integrity of high temperature welds, Nottingham, 1998. p. 355–70, IoM/IMech E.
[14] Fookes AJ, Smith DJ. Using a strain based failure assessment diagram for creep-brittle materials. Int J Pressure Vessels Piping 2001;78:951–61.
[15] Ainsworth RA. The treatment of thermal and residual stresses in fracture assessments. Engng Fract Mech 1986;24:65–76.
[16] Dong P, Hong JK. Recommendations for determining residual stresses in fitness-for-service assessment. Welding Research Council, New York, Bulletin 476, 2002.
[17] Ainsworth RA. Methods for treating displacement-controlled loading using the R6 defect assessment procedure. Nuclear Electric Report TD/SE/REP/0018, Berkeley Technology Centre, Berkeley, 1993.
[18] Ainsworth RA. The assessment of defects in structures of strain hardening material. Engng Fract Mech 1994;19:633–42.
[19] Goodall IW, Webster GA. Theoretical determination of reference stress for partially penetrating flaws in plates. Int J Pressure Vessels Piping 2001;78:687–95.
[20] Turner CE. Further developments of a *J*-based design curve and its relationship to other procedures. ASTM STP, 803II. Philadelphia: ASTM; 1983. p. 80–102.
[21] Blackburn WS. Assessment of cracks under secondary and combined loading. Int J Pressure Vessels Piping 1986;26:213–60.
[22] Newman Jr JC, Raju IS. An empirical stress-intensity factor equation for the surface crack. Engng Fract Mech 1981;15:185–92.